Adaptive defect-correction methods for viscous incompressible flow problems

SIAM J. NUMER. ANAL.
Vol. 37, No. 4, pp. 1165–1185

ADAPTIVE DEFECT-CORRECTION METHODS FOR VISCOUS INCOMPRESSIBLE FLOW PROBLEMS*

V. J. ERVIN†, W. J. LAYTON‡, AND J. M. MAUBACH‡

Abstract. We consider a defect correction method (DCM) which has been used extensively in applications where solutions have sharp transition regions, such as high Reynolds number fluid flow problems. A reliable a posteriori error estimator is derived for a defect correction method. The estimator is further studied for two examples: (a) the case of a linear-diffusion, nonlinear convection-reaction equation, and (b) the nonlinear Navier–Stokes equations. Numerical experiments are provided which illustrate the utility of the resulting adaptive defect correction method for high Reynolds number, incompressible, viscous flow problems.

Key words. defect correction, Navier–Stokes, finite element

AMS subject classifications. Primary, 65N30; Secondary, 76M10

PII. S0036142997318164

1. Introduction.

Defect-correction methods (DCMs) were originally viewed as alternates to Richardson extrapolation for increasing the formal order of finite difference methods. Increasingly, however, the development of the abstract theory for these procedures (see, e.g., [5], [6], [10], [18], [30], [22], [23], [34], [38]) as well as the computational practice of the methods (see, e.g., [17], [24], [25], [26], [27], [28]) have evolved to using defect correction to solve much harder, nearly singular, nonlinear problems through regularization and correction. This is somewhat surprising since solutions of representative applications such as high Reynolds number fluid flow problems [25], [26], [27], [28], [30], and convection-dominated, convection diffusion equations are characterized by sharp layers and transition regions. Thus, in spite of lacking the global smoothness required for the classical convergence analysis via asymptotic error expansions, global "uniform in epsilon" convergence in the smooth region has indeed been proven for defect correction methods in [5], [6], and [18] and experimentally verified [17], [24], [25], [26], [27], [28], even for these challenging applications.

For such problems, grid refinement in sharp transition regions is necessary in conjunction with the high accuracy attained in smooth regions by defect correction techniques. Reliability of the resulting self-adaptive, defect-correction procedure is then tied to the reliability of the a posteriori error estimator used for the defect-correction discretization. We consider precisely this issue herein.

Section 2 provides an a posteriori error estimator for DCMs for solving the general parameter dependent nonlinear problem $F(u\,,\epsilon) = 0$. The estimators are of the residual type for an abstract realization of the defect-correction discretization. They are further developed and particularized for two representative applications: linear diffusion coupled with nonlinear convection in section 3 and the incompressible Navier–Stokes equations (the targeted application) in section 4. Section 5 gives some

*Received by the editors March 7, 1997; accepted for publication (in revised form) September 26, 1998; published electronically March 23, 2000.
http://www.siam.org/journals/sinum/37-4/31816.html
†On leave from the Department of Mathematical Sciences, Clemson University, Clemson, SC 29634 (ervin@math.clemson.edu).
‡Institute for Computational Mathematics and Applications, Department of Mathematics and Statistics, University of Pittsburgh, Pittsburgh, PA 15260 (wjl+@pitt.edu). The second author was partially supported by NSF grants DMS-9400057, DMS-9972622, INT-9814115, and INT-9805563.

computational experiments with the resulting self-adaptive method.

To formulate the abstract problem, method, and results, let X and Y be Banach spaces $A \in \mathcal{L}(X, Y^*)$, $G(\cdot) \in C^1(X, Y^*)$, and $\epsilon \in \Lambda \subset \mathbb{R}$ Fréchet differentiable. The problem is now to solve

$$F(u, \epsilon) := A(\epsilon)u + G(u) = 0 \tag{1.1}$$

for $u = u(\epsilon)$. The abstract DCM is given as follows. Let $X_h, Y_h \subset X, Y$ (respectively) be finite dimensional subspaces and $A_h : X_h \to {Y_h}^*$, $G_h(\cdot) \in C^1(X_h, {Y_h}^*)$, be (finite dimensional) approximations of A and $G(\cdot)$, respectively.

Let $\epsilon_0 \geq \epsilon$, $A_h(\epsilon_0)$ be a "stabilized" or regularized approximation to $A_h(\epsilon)$, and let $J > 1$ be given. The method studied computes $u^1, \ldots, u^J \in X_h$ as follows: $u^1 \in X_h$ satisfies

$$F_h(u^1, \epsilon_0) := A_h(\epsilon_0)u^1 + G_h(u^1) = 0\,, \tag{1.2}$$

whereupon successive corrections are given by, for $j = 1, \ldots, J$,

$$A_h(\epsilon_0)u^{j+1} + G_h(u^{j+1}) = (A_h(\epsilon_0) - A_h(\epsilon))u^j\,. \tag{1.3}$$

There are numerous attractive practical features of (1.2), (1.3) cited in the above references. We take (1.2), (1.3) as the basic algorithm and work to find a computable upper bound for $||u - u^{j+1}||_X$. To realize (1.3), the iterand u^{j+1} is typically computed with a Newton method and is the root of $\hat{F}_{\epsilon_0}(u) = 0$ with $\hat{F}_{\epsilon_0}(u) := A_h(\epsilon_0)u + G_h(u) + (A_h(\epsilon) - A_h(\epsilon_0))u^j$. If the regularization is performed carefully, we often observe that only one or two Newton steps suffice in order to solve (1.3) for u^{j+1}, beginning with u^j, and that the resulting linearized systems are much cheaper to solve than are unregularized linear systems.

It is useful to think of (1.2) as an abstract realization of a convection-diffusion problem in which $A(\epsilon) \sim \epsilon A$. Suppose transition regions of the underlying physical problems are of width $\epsilon^{1/\alpha}$. Then a typical choice for $A_h(\epsilon_0)$ involves increasing, on each mesh cell, ϵ to $\epsilon + O$ (mesh cell diameter$^\alpha$) $\approx \epsilon + O(h^\alpha_{local})$, e.g., $\epsilon + O(h)$ for convection diffusion problems and $\epsilon + O(h^2)$ for $2d$ incompressible, viscous flow problems.

Herein we take an approach related to the local residual error estimators of [4], [7], [8], [9], [16], [19], and [43], as adapted to nonlinear problems in, e.g., [43] and [34]. In contrast to most of the work on error estimators for parameterized nonlinear equations, in which the goal is to construct reliably and efficiently the solution manifold as a function of the system parameter, the goal of defect–correction-type methods is to solve a nearly singular, very large, nonlinear system (such as high Reynolds number fluid flow [26], [27], [28], [29], [30]) via regularization by local effective viscosity adjustments followed by antidiffusion via correction.

2. Preliminaries. The basic assumption on (1.1) under which we proceed is that u is a nonsingular solution of (1.1), i.e., $DF(u, \epsilon) = [A(\epsilon) + DG(u)] \in \text{Isom}(X, Y^*)$, and that $DG(\cdot)$ is Lipschitz continuous in some ball about the solution u.

THEOREM 2.1. *Suppose that u is an isolated solution of* (1.1) *and that $DG(u)$ is Lipschitz continuous in some ball around u. Specifically, there is a $R_0 > 0$ such that*

$$\gamma := \sup_{w \in B(u; R_0)} \frac{||DG(w) - DG(u)||_{\mathcal{L}(X, Y^*)}}{||w - u||_X} < \infty\,.$$

Suppose that $u^j \in B(u;R)$, where

$$R := \min\left\{R_0,\, \gamma^{-1}||DF(u,\epsilon)^{-1}||^{-1}_{\mathcal{L}(Y^*,X)}\right\}. \tag{2.1}$$

Set $u^0 = 0$ and let u^j, $j = 1,\dots,J$, be given by (1.2), (1.3). Let $R_h \in \mathcal{L}(Y,Y_h)$ be a restriction operator. Then $||u-u^{j+1}||_X$ is bounded as follows:

For $j = 1,\dots,J-1$,

$$\begin{aligned}||u-u^{j+1}||_X \le 2||[A(\epsilon)+DG(u)]^{-1}||_{\mathcal{L}(Y^*,X)} \big\{&||(I_Y - R_h)^*\,[A(\epsilon)u^{j+1} + G(u^{j+1})]||_{Y^*}\\ &+ ||R_h||_{\mathcal{L}(Y,Y_h)}\,||(A(\epsilon)-A_h(\epsilon))u^{j+1} + (G-G_h)(u^{j+1})||_{Y_h^*}\\ &+ ||R_h||_{\mathcal{L}(Y,Y_h)}\,||(A_h(\epsilon_0)-A_h(\epsilon))\,(u^{j+1}-u^j)||_{Y_h^*}\Big\}.\end{aligned} \tag{2.2}$$

Proof. For R given by (2.1), and $w \in B(u,R) \subset X$,

$$w-u = DF(u,\epsilon)^{-1}\left\{F(w,\epsilon) + \int_0^1 [DF(u,\epsilon) - DF(u+t(w-u),\epsilon)](w-u)\,dt - F(u,\epsilon)\right\}.$$

Therefore (as $F(u,\epsilon)=0$),

$$\begin{aligned}||w-u||_X &\le ||DF(u,\epsilon)^{-1}||_{\mathcal{L}(Y^*,X)}\left\{||F(w,\epsilon)-F(u,\epsilon)||_{Y^*}\right.\\ &\qquad\left.+\int_0^1 ||DF(u,\epsilon) - DF(u+t(w-u),\epsilon)||_{\mathcal{L}(X,Y^*)}||w-u||_X\,dt\right\}\\ &\le ||DF(u,\epsilon)^{-1}||_{\mathcal{L}(Y^*,X)}\,||A(\epsilon)w + G(w)||_{Y^*}\\ &\qquad+\frac{1}{2}||DF(u,\epsilon)^{-1}||_{\mathcal{L}(Y^*,X)}\ \gamma\,||w-u||_X^2.\end{aligned}$$

By assumption on R, $||DF(u,\epsilon)^{-1}||_{\mathcal{L}(Y^*,X)}\,\gamma\,||w-u||_X \le ||DF(u,\epsilon)^{-1}||_{\mathcal{L}(Y^*,X)}\gamma\cdot R \le 1$. Thus,

$$||w-u||_X \le ||DF(u,\epsilon)^{-1}||_{\mathcal{L}(Y^*,X)}||A(\epsilon)w + G(w)||_{Y^*} + \frac{1}{2}||w-u||_X$$

and therefore,

$$\begin{aligned}||w-u||_X &\le 2||DF(u,\epsilon)^{-1}||_{\mathcal{L}(Y^*,X)}\ ||A(\epsilon)w + G(w)||_{Y^*}\\ &\le 2||DF(u,\epsilon)^{-1}||_{\mathcal{L}(Y^*,X)}\ ||F(w,\epsilon)||_{Y^*}.\end{aligned}$$

The next step is to let $w := u^{j+1}$ and to use its determining equations (1.2), (1.3). To this end, consider

$$\begin{aligned}||F(u^{j+1},\epsilon)||_{Y^*} &= \sup_{\phi\in Y}\frac{\langle A(\epsilon)u^{j+1} + G(u^{j+1}),\,\phi\rangle}{||\phi||_Y}\\ &= \sup_{\phi\in Y}\Big\{\langle A(\epsilon)u^{j+1} + G(u^{j+1}),\,\phi - R_h\phi\rangle\\ &\qquad - \langle (A_h(\epsilon)-A(\epsilon))u^{j+1} + (G_h-G)(u^{j+1}),\,R_h\phi\rangle\\ &\qquad + \langle (A_h(\epsilon_0)-A_h(\epsilon))(u^{j+1}-u^j),\,R_h\phi\rangle\Big\}/||\phi||_Y.\end{aligned}$$

As, $R_h \in \mathcal{L}(Y, Y_h)$, it follows immediately that

$$\begin{aligned}||F(u^{j+1},\epsilon)||_{Y^*} \leq\ & ||(I_Y - R_h)^*\,(A(\epsilon)u^{j+1} + G(u^{j+1}))||_{Y^*} \\ & + ||R_h||_{\mathcal{L}(Y,Y_h)}\,||(A(\epsilon) - A_h(\epsilon))u^{j+1} + (G - G_h)(u^{j+1})||_{Y_h^*} \\ & + ||R_h||_{\mathcal{L}(Y,Y_h)}\,||(A_h(\epsilon_0) - A_h(\epsilon))(u^{j+1} - u^j)||_{Y_h^*}\,,\end{aligned}$$

which completes the proof. □

Remark 2.1. The terms $A(\epsilon) - A_h(\epsilon)$ and $G - G_h$, represent consistency error terms and will normally be of higher order. Thus the error estimator will normally be dominated by the residual term $||(I_Y - R_h)^*\,(A(\epsilon)u^{j+1} + G(u^{j+1}))||_{Y^*}$ and the update $||(A_h(\epsilon_0) - A_h(\epsilon))(u^{j+1} - u^j)||_{Y_h^*}$. One example in which consistency error terms can be significant is when G_h includes terms arising from a subgridscale model added to the basic discretization.

3. A posteriori error estimators for a linear diffusion–nonlinear convection problem. Let $\Omega \subset \mathbb{R}^2$, $X = Y := \overset{o}{W}{}^{1,2}(\Omega)$. Set $||u||_X = ||\nabla u||_{L^2(\Omega)}$ and define $F(u,\epsilon)$ via the Riesz representation theorem as the element of X^* satisfying

$$\langle F(u,\epsilon)\,,\,\phi\rangle := \int_\Omega [\epsilon \nabla u \cdot \nabla\phi + g(\nabla u, u)\phi - f\phi]\,dx\,. \tag{3.1}$$

Then, u is a solution of $F(u,\epsilon) = 0$ in X if and only if u is a weak solution of the convection-diffusion-reaction equation:

$$\begin{cases} -\epsilon\triangle u + g(\nabla u, u) = f \text{ in } \Omega \subset \mathbb{R}^2\,, \\ \qquad\qquad u = 0 \text{ on } \partial\Omega\,. \end{cases}$$

Let $X_h = Y_h \subset X$ be a conforming finite element space (assuming Ω is a polygonal domain), for specificity, and suppose X_h contains C^0 piecewise polynomials of degree $\leq k$ on an edge-to-edge triangulation of $\Pi^h(\Omega)$ of Ω. The triangulation, $\Pi^h(\Omega)$, is assumed to have its "minimum angle" $\theta_{min}(\Pi^h(\Omega))$ bounded away from zero uniformly in h; see, e.g., [45] for more details on these conditions.

The usual Galerkin finite element approximation of (3.1) is given by $F_h(w_h,\epsilon) = 0 \in X_h^*$ where, for all w_h, $\phi_h \in X_h$,

$$\langle F_h(w_h,\epsilon)\,,\phi_h\rangle = \langle F(w_h,\epsilon)\,,\phi_h\rangle\,.$$

The operators A_h , $G_h(\cdot)$ are defined analogously to $F(\cdot,\cdot)$ via the Riesz representation theorem and the relations:

$$\langle A_h(\epsilon)w_h\,,\,\phi_h\rangle = \int_\Omega \epsilon\,\nabla w_h \cdot \nabla\phi_h\,dx\,,$$

$$\langle A_h(\epsilon_0)w_h\,,\,\phi_h\rangle = \sum_{T\in\Pi^h(\Omega)} \int_T (\epsilon + diam(T))\,\nabla w_h \cdot \nabla\phi_h\,dx\,,$$

$$\langle G_h(w_h)\,,\,\phi_h\rangle = \int_\Omega [g(\nabla w_h, w_h)\phi_h - f\phi_h]\,dx\,.$$

With these choices of F_h, A_h, and G_h, (1.2), (1.3) becomes the usual finite element, defect-correction discretization of (3.1).

Provided, e.g., $g(s,t)$ satisfies a growth condition and $\int_\Omega g(\nabla w, w)\, w\, dx \geq 0$ for $w \in X$, it can be shown that weak solutions of $F(u,\epsilon) = 0$ (3.1) exist. If $F(u,\epsilon)$ is monotone as a function of u, solutions are also unique. (In the linear case, $g(\nabla w, w) = \mathbf{b}\cdot\nabla w + pw$, and this holds if $p - 1/2\,\nabla\cdot\mathbf{b} \geq 0$.) We assume that, minimally, the solution u we approximate is nonsingular in the sense that $D_u F(u,\epsilon)$ is invertible.

We also suppose that the finite element space admits the existence of an interpolation operator R_h of the Clément type. Specifically, $R_h\colon X \mapsto X_h$ satisfies the following elementwise error estimate (see [12]). For $\phi \in X$ there are $C_i = C_i(\theta_{min}(\Pi^h(\Omega)))$, $i = 1,2,3$, such that

$$\left.\begin{array}{c} ||\phi - R_h\phi||_{W^{j-1,2}(T)} \leq C_1 h_T^{2-j} ||\phi||_{W^{1,2}(N(T))}\,,\ j = 1,2\,, \\ ||\phi - R_h\phi||_{L^2(T)} \leq C_2 ||\phi||_{L^2(N(T))}\,, \\ ||\phi - R_h\phi||_{L^2(e)} \leq C_3 h_e^{1/2} ||\phi||_{W^{1,2}(N(e))}\,, \end{array}\right\} \tag{3.2}$$

for all elements $T \in \Pi^h(\Omega)$ and all edges e of the elements. Here $N(T)$ and $N(e)$ denote the union of all the elements touching T and e, respectively. Also h_e and h_T will denote, as usual, the diameters of an edge e and element T, respectively.

For the first term on the right-hand side of (2.2) we have, for $\phi \in Y$, $||\phi||_Y = 1$,

$$\begin{aligned} \left\langle (I_Y - R_h)^* \left[A(\epsilon)u^{j+1} + G(u^{j+1})\right], \phi \right\rangle &= \left\langle A(\epsilon)u^{j+1} + G(u^{j+1}), \phi - R_h\phi \right\rangle \\ &= \sum_{T\in\Pi^h(\Omega)} \int_T \epsilon\nabla u^{j+1}\cdot\nabla(\phi - R_h\phi) + [g(\nabla u^{j+1}, u^{j+1}) - f](\phi - R_h\phi)\, dx\,. \end{aligned}$$

Integration by parts over each $T \in \Pi^h(\Omega)$ and denoting the collection of interior edges in $\Pi^h(\Omega)$ by $E^h(\Omega)$, with the use of estimates like

$$\sum_T ||r^{j+1}||_{L^2(T)} ||\phi||_{W^{1,2}(N(T))} \leq C \left(\sum_T ||r^{j+1}||^2_{L^2(T)} \right)^{1/2} ||\phi||_{W^{1,2}(\Omega)}\,,$$

yields

$$\begin{aligned} &\left\langle (I_Y - R_h)^* \left[A(\epsilon)u^{j+1} + G(u^{j+1})\right], \phi \right\rangle \\ &= \sum_{T\in\Pi^h(\Omega)} \int_T (-\epsilon\triangle u^{j+1} + g(\nabla u^{j+1}, u^{j+1}) - f)\,(\phi - R_h\phi)\, dx \\ &\quad + \sum_{e\in E^h(\Omega)} \int_e \epsilon(\nabla u^{j+1}\cdot\mathbf{n}_e)\,(\phi - R_h\phi)\, de \\ &\leq C_1 \sum_{T\in\Pi^h(\Omega)} ||r^{j+1}||_{L^2(T)}\, h_T\, ||\phi||_{W^{1,2}(N(T))} \\ &\quad + C_2\,\epsilon \sum_{e\in E^h(\Omega)} ||[\nabla u^{j+1}\cdot\mathbf{n}_e]_e||_{L^2(e)}\, h_e^{1/2}\, ||\phi||_{W^{1,2}(N(e))} \\ &\leq C \left\{ \sum_{T\in\Pi^h(\Omega)} h_T^2\, ||r^{j+1}||^2_{L^2(T)} + \epsilon^2 \sum_{e\in E^h(\Omega)} h_e\, ||[\nabla u^{j+1}\cdot\mathbf{n}_e]_e||^2_{L^2(e)} \right\}^{1/2} ||\phi||_{W^{1,2}(\Omega)}\,, \end{aligned}$$

where r^{j+1} is the residual, defined per mesh element T by $r^{j+1} := f - (-\epsilon\triangle u^{j+1} + g(\nabla u^{j+1}, u^{j+1}))$, $C = C(C_1, C_2, \theta_{min}(\Pi^h(\Omega)))$ is a computable constant, and $[u]_e$ denotes the jump of u across edge e.

With the usual conforming finite element formulation specified in this example, the second term in the right-hand side of (2.2) is identically zero. To see this, note that for all $\phi_h \in Y_h$, $\left\langle F(u^{j+1}, \epsilon)\,,\, \phi_h \right\rangle = \left\langle F_h(u^{j+1}, \epsilon)\,,\, \phi_h \right\rangle$, so that

$$\begin{aligned} ||(A(\epsilon) - A_h(\epsilon))u^{j+1} + (G - G_h)(u^{j+1})||_{Y_h{}^*} \\ &= \sup_{\phi_h \in Y_h} \left\langle (A(\epsilon) - A_h(\epsilon))u^{j+1} + (G - G_h)(u^{j+1})\,,\, \phi_h \right\rangle \\ &= \sup_{\phi_h \in Y_h} \left\langle F(u^{j+1}, \epsilon) - F_h(u^{j+1}, \epsilon)\,,\, \phi_h \right\rangle = 0\,. \end{aligned}$$

As for the last term, let $\phi_h \in Y_h$, $||\phi_h||_Y = 1$. Then,

$$\begin{aligned} \left\langle (A_h(\epsilon_0) - A_h(\epsilon))\,(u^{j+1} - u^j)\,, \phi_h \right\rangle &= \int_\Omega (\epsilon_0 - \epsilon)\,\nabla(u^{j+1} - u^j) \cdot \nabla\phi_h \, dx \\ &\le \left[\sum_{T \in \Pi^h(\Omega)} ||(\epsilon_0 - \epsilon)\,\nabla(u^{j+1} - u^j)||^2_{L^2(T)} \right]^{1/2}. \end{aligned}$$

Combining these terms gives the following error estimate for the method (1.2), (1.3) applied to the convection-diffusion-reaction problem:

$$\begin{aligned} ||u - u^{j+1}||_{W^{1,2}(\Omega)} \le C\,||DF(u,\epsilon)^{-1}||_{\mathcal{L}(Y^*,X)} \Bigg\{ & \sum_{T \in \Pi^h(\Omega)} h_T^2\,||r^{j+1}||^2_{L^2(T)} \\ & + \epsilon^2 \sum_{e \in E^h(\Omega)} h_e\,||[\nabla u^{j+1} \cdot \mathbf{n}_e]_e||^2_{L^2(e)} \\ & + \sum_{T \in \Pi^h(\Omega)} ||\,(\epsilon_0 - \epsilon)\,\nabla(u^{j+1} - u^j)\,||^2_{L^2(T)} \Bigg\}^{1/2}. \end{aligned} \tag{3.3}$$

In order to ensure full reliability, it remains to estimate $||DF(u,\epsilon)^{-1}||_{\mathcal{L}(Y^*,X)}$. This depends of course upon the precise nonlinearity $g(\nabla u, u)$. In general, $g(\nabla u, u)$ and $||DF(u,\epsilon)^{-1}||_{\mathcal{L}(Y^*,X)}$ can be approximated by $||DF(u^{j+1},\epsilon)^{-1}||_{\mathcal{L}(Y_h^*,X_h)}$. (This involves the solution of an eigenvalue problem.) In some cases this multiplier can be bounded analytically. To illustrate this, let us assume that $g(\nabla w, w) = f + \underline{b}\cdot\nabla w + pw$, where $p - \nabla\cdot\underline{b}/2 \ge p_0 > 0$. Under this assumption a solution ϕ to $A(\epsilon)\phi + G(\phi) = 0$ exists for any $f \in Y^*$. Straightforward manipulations immediately give

$$\epsilon||\nabla\phi||_{L^2(\Omega)} \le C||f||_{W^{2,-1}(\Omega)}$$

so that, in this case of a linear problem,

$$||DF(u,\epsilon)^{-1}||_{\mathcal{L}(Y^*,X)} \le C\epsilon^{-1}\,.$$

However, in the most interesting cases this common multiplier must be approximated (as noted above), or estimated in an ad hoc way via data-fitting.

4. Application to the Navier–Stokes equations. Let $d = 2, 3$ be the dimension of a polygonal domain Ω. Define $X = Y := ((\overset{o}{W}{}^{1,2}(\Omega))^d, L_0^2(\Omega))$, where $L_0^2(\Omega)$ is the space of $L^2(\Omega)$ functions with zero mean. The norm of $\tilde{\mathbf{u}} = (\mathbf{u}, p) \in X$ is given by

$$\|\tilde{\mathbf{u}}\|_X := [\|\nabla \mathbf{u}\|^2_{L^2(\Omega)} + \|p\|^2_{L^2(\Omega)}]^{1/2}.$$

Define, via the Riesz representation theorem, $F(\tilde{\mathbf{u}}, \epsilon)$ as that element of X^* satisfying

$$\langle F(\tilde{\mathbf{u}}, \epsilon), \tilde{\mathbf{v}} \rangle = \int_\Omega [\, \epsilon \, \nabla \mathbf{u} : \nabla \mathbf{v} + \mathbf{u} \cdot \nabla \mathbf{u} \cdot \mathbf{v} + q \nabla \cdot \mathbf{u} - p \nabla \cdot \mathbf{v} - \mathbf{f} \cdot \mathbf{v}] \, dx \text{ for all } \tilde{\mathbf{v}} \in X,$$

where $\epsilon = \mathrm{Re}^{-1}$ is the inverse of the Reynolds number, $\tilde{\mathbf{u}} = (\mathbf{u}, p) \in X$ and $\tilde{\mathbf{v}} = (\mathbf{v}, q) \in X$.

The problem of solving $F(\tilde{\mathbf{u}}, \epsilon) = 0$ for $\tilde{\mathbf{u}} \in X$ is the equivalent to that of finding the weak solution $\tilde{\mathbf{u}} = (\mathbf{u}, p) \in X$ to the Navier–Stokes equations with $\epsilon = \mathrm{Re}^{-1}$:

$$\left.\begin{aligned} -\mathrm{Re}^{-1} \triangle \mathbf{u} + \mathbf{u} \cdot \nabla \mathbf{u} + \nabla p = \mathbf{f} \text{ in } \Omega, \ \mathbf{u} = \mathbf{0} \text{ on } \partial\Omega, \\ \nabla \cdot \mathbf{u} = g \text{ in } \Omega, \ \textstyle\int_\Omega p \, dx = 0. \end{aligned}\right\} \tag{4.1}$$

Given an edge to edge triangulation of Ω, $\Pi^h(\Omega)$, whose minimum angle θ_{min} is bounded away from zero, velocity-pressure finite element spaces can then be constructed on $\Pi^h(\Omega)$. We assume that each possesses an interpolation operator of the Clément type satisfying (3.2). See [12] and [20] for examples.

Let (V^h, Q^h) denote those velocity-pressure finite element spaces which are assumed additionally to satisfy the inf-sup (or Babuska–Brezzi) condition [20], [21]. Specifically, there is a $\beta > 0$, independent of h, such that

$$\inf_{0 \neq q \in Q^h} \sup_{\mathbf{0} \neq \mathbf{v} \in V^h} \frac{\int_\Omega q \, \nabla \cdot \mathbf{v} \, dx}{\|\nabla \mathbf{v}\|_{L^2(\Omega)} \, \|q\|_{L^2(\Omega)}} \geq \beta > 0. \tag{4.2}$$

The usual Galerkin-finite element approximation to (4.1) is then given by $F_h(\tilde{\mathbf{u}}^h, \epsilon) = 0$ where, for all $\tilde{\mathbf{w}}_h, \tilde{\phi}_h \in X^h := (V^h, Q^h)$, $F_h(\cdot, \cdot)$ is defined by

$$\langle F_h(\tilde{\mathbf{w}}_h, \epsilon), \tilde{\phi}_h \rangle := \langle F(\tilde{\mathbf{w}}_h, \epsilon), \tilde{\phi}_h \rangle.$$

A_h and G_h are defined analogously to section 3 by

$$\langle A_h(\epsilon) \tilde{\mathbf{w}}_h, \tilde{\phi}_h \rangle := \sum_{T \in \Pi^h(\Omega)} \int_T \epsilon \, \nabla \mathbf{w}_h : \nabla \phi_h \, dx,$$

$$\langle G_h(\tilde{\mathbf{w}}_h), \tilde{\phi}_h \rangle := \langle F_h(\tilde{\mathbf{w}}_h, \epsilon) - A_h(\epsilon) \tilde{\mathbf{w}}_h, \tilde{\phi}_h \rangle,$$

where $\tilde{\mathbf{w}}_h = (\mathbf{w}_h, q) \in X^h$, $\tilde{\phi}_h := (\phi_h, \lambda) \in X^h$.

With these choices of A_h, ϵ, $\epsilon_0(T) := \max\{\epsilon, h_T\}$ and $G_h(\cdot)$, (1.2), (1.3) reduces to the usual finite element, nonlinear defect-correction discretization of the incompressible Navier–Stokes equations (see, e.g., [20] and [21]). It is often highly advantageous in the algorithm to perturb $G_h(\cdot)$ through local averaging or the use of "flux limiters" (see [26], [27], [28]) or through the incorporation of an appropriate subgridscale model.

For example, the incorporation of the model suggested in [31] (which is used herein) is equivalent to defining $G_h(\cdot)$ as

$$\begin{aligned}\langle G_h(\tilde{\mathbf{w}}_h), \tilde{\phi}_h\rangle := \langle F_h(\tilde{\mathbf{w}}_h, \epsilon) - A_h(\epsilon)\tilde{\mathbf{w}}_h\,,\, \tilde{\phi}_h\rangle \\ + \langle \mu(h, Re)\,|\nabla \mathbf{w}_h|^r \nabla \mathbf{w}_h\,,\, \nabla \phi_h\rangle\,,\end{aligned}$$

where the scaling term $\mu(h, \mathrm{Re})$ and exponent r are discussed in [31]. This incorporation adds one additional term to the right-hand side of the error estimator but does not otherwise appreciably alter the following analysis. Let $\tilde{\phi} \in Y$, $\|\tilde{\phi}\|_Y = 1$ be given and consider the first term on the right-hand side of (2.2):

$$\begin{aligned}&\langle (I_Y - \tilde{R}_h)^*[A(\epsilon)\tilde{\mathbf{u}}^{j+1} + G(\tilde{\mathbf{u}}^{j+1})]\,,\, \tilde{\phi}\rangle = \langle A(\epsilon)\tilde{\mathbf{u}}^{j+1} + G(\tilde{\mathbf{u}}^{j+1})\,,\, \tilde{\phi} - \tilde{R}_h\tilde{\phi}\rangle \\ &= \sum_{T\in\Pi^h(\Omega)} \int_T [\,\epsilon\,\nabla \mathbf{u}^{j+1} : \nabla(\phi - R_h^V\phi) + \mathbf{u}^{j+1}\cdot\nabla\mathbf{u}^{j+1}\cdot(\phi - R_h^V\phi) \\ &\qquad + (q - R_h^Q q)\nabla\cdot\mathbf{u}^{j+1} \\ &\qquad -p^{j+1}\nabla\cdot(\phi - R_h^V\phi) - g\cdot(q - R_h^Q q) - \mathbf{f}\cdot(\phi - R_h^V\phi)\,]\,dx,\end{aligned}$$

where $\tilde{\phi} = (\phi, q)$. Integration by parts over each $T \in \Pi^h(\Omega)$ and denoting the collection of faces (3-D) or edges (2-D) of $\Pi^h(\Omega)$ in the interior of Ω by $E^h(\Omega)$ give

$$\begin{aligned}&\langle (I_Y - \tilde{R}_h)^*[A(\epsilon)\tilde{\mathbf{u}}^{j+1} + G(\tilde{\mathbf{u}}^{j+1})]\,,\, \tilde{\phi}\rangle \\ &\quad = \sum_{T\in\Pi^h(\Omega)} \int_T -\mathbf{r}^{j+1}\cdot(\phi - R_h^V\phi) + \int_T (q - R_h^Q q)(\nabla\cdot\mathbf{u}^{j+1} - g)\,dx \\ &\quad + \sum_{e\in E^h(\Omega)} \int_e \epsilon\,[\nabla\mathbf{u}^{j+1}\cdot\mathbf{n}_e]_e\cdot(\phi - R_h^V\phi) - [p^{j+1}]_e\,(\phi - R_h^V\phi)\cdot\mathbf{n}_e\,d\sigma\,,\end{aligned}$$

where $\mathbf{r}^{j+1} := \mathbf{f} - (-\mathrm{Re}^{-1}\triangle\mathbf{u}^{j+1} + \mathbf{u}^{j+1}\cdot\nabla\mathbf{u}^{j+1} + \nabla p^{j+1})$.

Using the Cauchy–Schwarz inequality on each element T and face (or edge) e and the properties of $\tilde{R}_h\phi$ from (3.2) gives

$$\begin{aligned}&\langle (I_Y - \tilde{R}_h)^*[A(\epsilon)\tilde{\mathbf{u}}^{j+1} + G(\tilde{\mathbf{u}}^{j+1})]\,,\, \tilde{\phi}\rangle \le \\ &\quad C\left[\sum_{T\in\Pi^h(\Omega)} h_T^2\|\mathbf{r}^{j+1}\|_{0,T}^2 + \|\nabla\cdot\mathbf{u}^{j+1} - g\|_{0,T}^2\right]^{1/2} \\ &\quad + C\left[\sum_{e\in E^h(\Omega)} h_e\,\|[\mathrm{Re}^{-1}\nabla\mathbf{u}^{j+1}\cdot\mathbf{n}_e - p^{j+1}\mathbf{n}_e]_e\|_{0,e}^2\right]^{1/2},\end{aligned}$$

which is a bound on the first term on the right-hand side of (2.2).

If the usual Galerkin formulation is used (i.e., no "subgridscale" modelling, numerical integration, or other variational crime) then, as in the previous example, the second term on the right-hand side of (2.2) is identically zero. As for the last term which involves $A_h(\epsilon_0) - A_h(\epsilon)$, let $\tilde{\phi} \in Y$ satisfy $\|\tilde{\phi}\|_Y = 1$. Then,

$$\langle (\, A_h(\epsilon_0) \,-\, A_h(\epsilon)\,)(\tilde{\mathbf{u}}^{j+1} - \tilde{\mathbf{u}}^{j}\,), \tilde{\phi}\rangle = \int_\Omega (\epsilon_0 \,-\, \epsilon)\, \nabla(\mathbf{u}^{j+1} \,-\, \mathbf{u}^{j}) : \nabla\phi \, dx$$

$$\leq \left[\sum_{T\in\Pi^h(\Omega)} \|(\epsilon_0(T) \,-\, \epsilon)\, \nabla(\mathbf{u}^{j+1} \,-\, \mathbf{u}^{j})\|_{0,T}^2 \right]^{1/2}.$$

Combining these terms gives an error estimator:

$$\begin{aligned}
&\|\mathbf{u} \,-\, \mathbf{u}^{j+1}\|_1 \,+\, \|p \,-\, p^{j+1}\| \\
&\quad \leq C\, \|DF(\tilde{\mathbf{u}}, \epsilon)^{-1}\|_{\mathcal{L}(Y^*,X)} \left\{ \sum_{T\in\Pi^h(\Omega)} h_T^2 \|\mathbf{r}^{j+1}\|_{0,T}^2 \,+\, ||\nabla\cdot\mathbf{u}^{j+1} - g||_{0,T}^2 \right. \\
&\quad + \sum_{e\in E^h(\Omega)} h_e\, \|[\mathrm{Re}^{-1}\nabla\mathbf{u}^{j+1}\cdot\mathbf{n}_e \,-\, p^{j+1}\mathbf{n}_e]_e\|_{0,e}^2 \\
&\quad \left. + \sum_{T\in\Pi^h(\Omega)} \|(\epsilon_0(T) \,-\, \epsilon)\, \nabla(\mathbf{u}^{j+1} \,-\, \mathbf{u}^{j})\|_{0,T}^2 \right\}^{1/2}.
\end{aligned}$$

Remark 4.1. If the aforementioned subgridscale model from [31] is used in the residual calculation, then an extra term appears on the right-hand side. This term takes the form

$$\left[\sum_{T\in\Pi^h(\Omega)} ||\mu(h_T, \mathrm{Re})|\nabla\mathbf{u}^j|^p \nabla\mathbf{u}^j||_{L^2(T)}^2 \right]^{1/2}.$$

It remains, of course, to evaluate $\|DF(\tilde{\mathbf{u}}, \epsilon)^{-1}\|_{\mathcal{L}(Y^*,X)}$. The Navier–Stokes equations are not monotone so an a priori bound of this term for all possible solutions is not possible. (Singular solutions *do* exist and correspond to physically interesting flow situations.) Since $\|DF(\tilde{\mathbf{u}}, \epsilon)^{-1}\|_{\mathcal{L}(Y^*,X)}$ is a common multiplier of the right-hand side of (4.3), it is not required for mesh redistribution, only for the computation of a reliable upperbound in order to check if a final stopping criterion is satisfied. Unfortunately, in general, this multiplier can only be estimated by, e.g., solving an eigenvalue problem on a course mesh. This amounts to replacing $\|DF(\tilde{\mathbf{u}}, \epsilon)^{-1}\|_{\mathcal{L}(Y^*,X)}$ by $\|DF(\tilde{\mathbf{u}}^{j+1}, \epsilon)^{-1}\|_{\mathcal{L}(X^{H*},X^H)}$, where $H >> h$.

5. Numerical results. We give an illustration of the effectiveness of using defect correction methods, with a subgridscale (SGS) model, in an adaptive calculation. To illustrate the method we solve an equilibrium, high Reynolds number flow problem (4.9) via the DCM presented in section 1. In the tests presented herein, we use either the $k = 1$ accurate minielement (Arnold, Brezzi, and Fortin [1]) or the second order $k = 2$ accurate Taylor–Hood pair [40].

The nonlinear systems arising at each step of the method, denoted $F(x) = 0$, were linearized by a damped inexact Newton method [14], with stopping criterion $||F(x)||_2 < 10^{-8}$. The resulting nonsymmetric linearized systems were solved with Sonneveld's [37] conjugate gradient squared (CGS) (with a Vanka-like ILU(0) preconditioner [42]). The generalized minimal residual method (GMRES) of Saad and Schultz [36] or Axelsson's generalized conjugate gradient least squares method (GCGLS) [2], [3] can also be used. However, it is our experience that they can consume more computational time because they explicitly orthogonalize search directions.

The storage of more search directions further limits the number of degrees of freedom which can be handled. The pressure was normalized by fixing its value at one point of the domain.

The initial guess for calculations on each newly refined grid is the solution interpolated from the previous grid. Grid to grid interpolation is easy because the grid refinement employed (see [32]) is hierarchical with conforming basis functions. Thus, the hierarchical mesh levels automatically provide accurate initial guesses to the nonlinear solver. The few nonlinear iterations (Newton steps) required reflects both this good initial guess and regularization of the system inherent in DCMs.

We have purposely used the most conservative options at each step because we are testing the viability of the basic DCM, rather than the many possible efficiency improvements. For example, the linear and nonlinear systems were solved to essentially machine precision (rather than truncation error of the step in question). For the same reason, on each new mesh, the DCM was restarted by solving an artificial viscosity approximation followed by the corrections.

For every grid, first the artificial viscosity system (1.2) was solved, with $\epsilon_0 = \epsilon + h^\alpha$. Next, k (the polynomial degree of the velocity approximation) antidiffusive defect corrections steps (1.3) follow. Thus one defect-correction iteration was used for the minielement, and two iterations were used for the Taylor–Hood pair.

The stopping criterion used was $||r^{(l)}||_2 < 10^{-11}$, where $r^{(l)}$ is the lth *updated residual*. In all examples, the nodes were numbered left to right and bottom to top. As usual, the $ILU(0)$ preconditioner performs best for lower degree polynomial velocity approximations, when mesh refinement is limited and when nodal support points are numbered regularly. In spite of this, we experienced no difficulties using a simple ILU(0) preconditioner, because the linear systems we solved arose from a regularized artificial viscosity approximation.

The coefficients of the discrete systems were computed with quadrature rules of degree $2k$. All quadrature rules employed use quadrature points strictly inside the reference element. In the case of $k = 1$, for instance, we used rule "T_2: 5-1" of degree 5 from Stroud [39, p. 314]. For higher polynomial degree k, quadrature formulas were taken from Dunavant [15]. The jump integrals over the edges, were computed with a standard Gauss–Legendre formula which is exact for all polynomials of degree $2k$.

All numerical experiments used the same mesh refinement technique. The coarse grids were of the Tucker–Whitney triangular type described by Todd [41]. The grid refinement algorithm of [32] and [33] was used to create the finer uniform and adaptively locally refined meshes.

The local error indicators were based on the estimator (4.3). For an element T, we measured the local error indicators, including a possible SGS model,

$$\begin{aligned} Est_\alpha^2(T) &= C_1^2 \left[h_T^2 \|\mathbf{r}^{j+1}\|_{0,T}^2 + ||\nabla \cdot \mathbf{u}^{j+1} - g\|_{0,T}^2 \right] \\ &\quad + C_2^2 \left[\sum_{e \in T} h_e \, \|[\mathrm{Re}^{-1} \nabla \mathbf{u}^{j+1} \cdot \mathbf{n}_e - p^{j+1} \mathbf{n}_e]_e\|_{0,e}^2 \right] \\ &\quad + C_3^2 \left[\|(\epsilon_0(T) - \epsilon) \nabla (\mathbf{u}^{j+1} - \mathbf{u}^j)\|_{0,T}^2 + ||\mu(h_T, Re) |\nabla \mathbf{u}^j|^p \nabla \mathbf{u}^j||_{0,T}^2 \right] . \end{aligned} \tag{5.1}$$

The local error indicators sum up to our global error estimate

$$Est_\alpha^2(\Omega) := \sum_{T \in \Pi^h(\Omega)} Est_\alpha^2(T). \tag{5.2}$$

TABLE 5.1
Estimated and actual energy norm error ratios for the DCM.

α	Est_α/Est_1	Err_α/Err_1
1	1.00	1.00
3/2	1.81	1.02
2	4.07	1.91

TABLE 5.2
Estimated and actual error ratios for the DCM.

α	Est_α/Est_1	Err_α/Err_1
1	1.00	1.00
3/2	1.06	0.90
2	1.41	1.20

The error indicator for T, $Est_\alpha(T)$, depends on the amount of artificial viscosity $\epsilon_0 - \epsilon =: h^\alpha$. Here we choose $\alpha > 0$, a real number, and $h = h_T$, the diameter of triangle T. The usual choice for convection diffusion problems (see [5], [18], [24], and [30]) is $\alpha = 1$. Since these problems have $O(\epsilon)$ layers for $2d$ flow problems we first tested this choice for the equilibrium Navier–Stokes equations. The optimal amount of artificial diffusion $h^\alpha = \epsilon_0 - \epsilon$ for the DCM is explored for the Navier–Stokes equations using an example of [29].

Test problem 5.1. On the domain $[0,1]^2$, we used for the exact solution $(\mathbf{u}, p)$

$$\mathbf{u}_1 = \sin \pi x \sin 2\pi x, \quad \mathbf{u}_2 = x^2(1-x)\sin \pi y, \quad p = (1 + y(y^2-4))\cos \pi x. \tag{5.3}$$

The right-hand side $f = f(x, y, Re)$ was obtained by substituting (5.3) into the Navier–Stokes equations. The velocity $\mathbf{u}$ satisfies the homogeneous Dirichlet boundary condition and is smooth uniformly in the Reynolds number.

We take $\mathrm{Re} = 10^4$, set $C_1 = C_2 = C_3 = 1$, and compute $Est^2_\alpha(\Omega)$ and the true error for the discretization using a Taylor–Hood finite element approximation. Rather than estimating the common multiplier $||DF^{-1}(\mathbf{u}, \epsilon)||$, we tabulated the ratios of the estimated errors $Est_\alpha(\Omega)/Est_1(\Omega)$ and the true errors $Err_\alpha(\Omega)/Err_1(\Omega)$. The first column of Table 5 shows the exponent α of our artificial viscosity parameter h^α. The second column shows the ratios $Est_\alpha(\Omega)/Est_1(\Omega)$ of the estimated errors, and the last column the ratios of the true errors.

The standard choice $\alpha = 1$ appears to be the best choice for globally smooth flow problems without transition regions.

Results from additional experiments for more physically interesting flow problems, without a known exact solution (hence only calculating the first column in the table), also suggest that the optimal artificial viscosity parameter was $O(h^1)$. A similar trend was observed if the minielement is used for the finite element discretization; see Table 5.2.

For Test Problem 5.1, the estimated error was an accurate estimate of the true error for our choice of constants C_j. For example, with the minielement

$$Est^2_1(\Omega)/Err^2_1(\Omega) \approx 0.51/0.50 \approx 1.02.$$

Table 5.2 is a clear case when energy norm optimization yields a different optimal value of α than optimizing the "eyeball" norm. For the latter case we obtained $\alpha = 2$ in Test Problem 5.2. We do not have a rigorous explanation of this discrepancy.

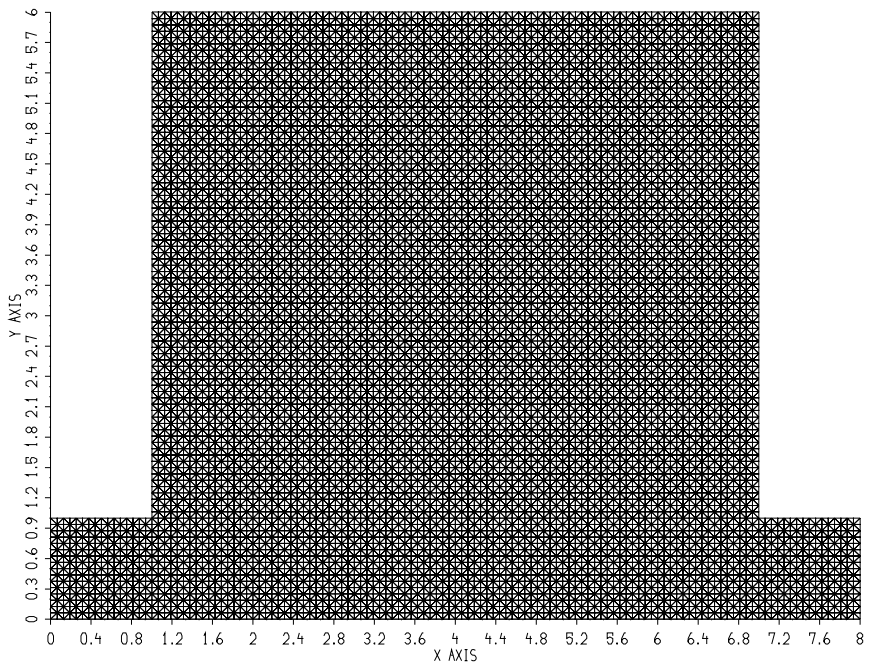

FIG. 5.1. *The uniform grid upon which the artificial viscosity parameter α is tested in Figures* 5.2–5.4.

Test problem 5.2. We solve the Navier–Stokes equations (4.1) with $f = 0$ and $g = 0$ (adapted from Mohammadi and Pironneau [35]).

The domain Ω of this pipe cavity flow problem is shown in Figure 5.5. The Reynolds number used was Reynolds number $\mathrm{Re} = (1.75 \cdot 10^{-5})^{-1}$ (see [13], [11], and [44]). The fluid flows in from the left with the standard parabolic profile $\mathbf{u}_1(x, y) = 4y(1 - y)$, $\mathbf{u}_2(x, y) = 4y(1 - y)$ along boundary $\{(x, y) : x = 0, y \in [0, 1]\}$ and out at the pipe's right end (with the same profile). The Dirichlet boundary conditions are homogeneous except for the pipe's inflow and outflow boundaries. (The tests in [11] use Neumann-type boundary conditions on the outflow boundary of the pipe; the physical validity of either outflow boundary conditions can be argued.)

Three interesting physical structures are expected at a higher Reynolds number: A large recirculating region in the cavity, a separation line near the cavity-pipe juncture, and very small recirculating eddy where the flow leaves the cavity to re-enter the pipe. The last two structures carry most of the vorticity of the flow field and the region below the separating line carries most of the momentum of the flow field. First we determine which order of artificial diffusion α gives the sharpest resolution of the transition regions and physical structures. The minielement was used to test resolution as a function of α together with the uniform grid in Figure 5.1 containing approximately 20,000 triangles. The flow fields are shown in Figures 5.2–5.4. The velocity vectors are rescaled to have the same length. Figure 5.2 indicates that a large amount of $O(h)$ artificial viscosity is undesirable. Indeed, the separation curve in the flow field computed with $\alpha = 2$, $O(h^2)$ artificial viscosity, presented in Figure 5.4, more closely resembles the separation curve calculated in [35]. For our tests with

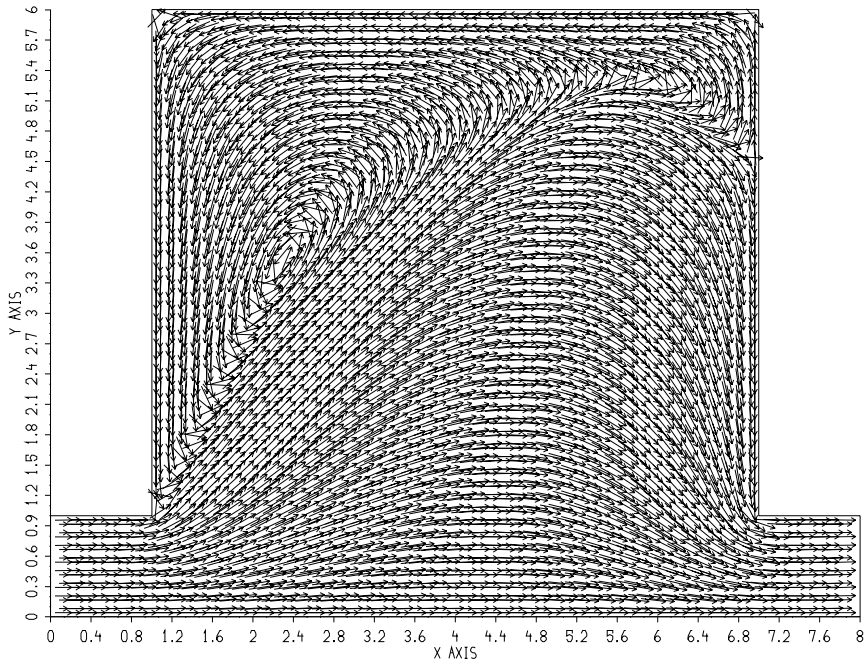

FIG. 5.2. *The $\alpha = 1$ flow field.*

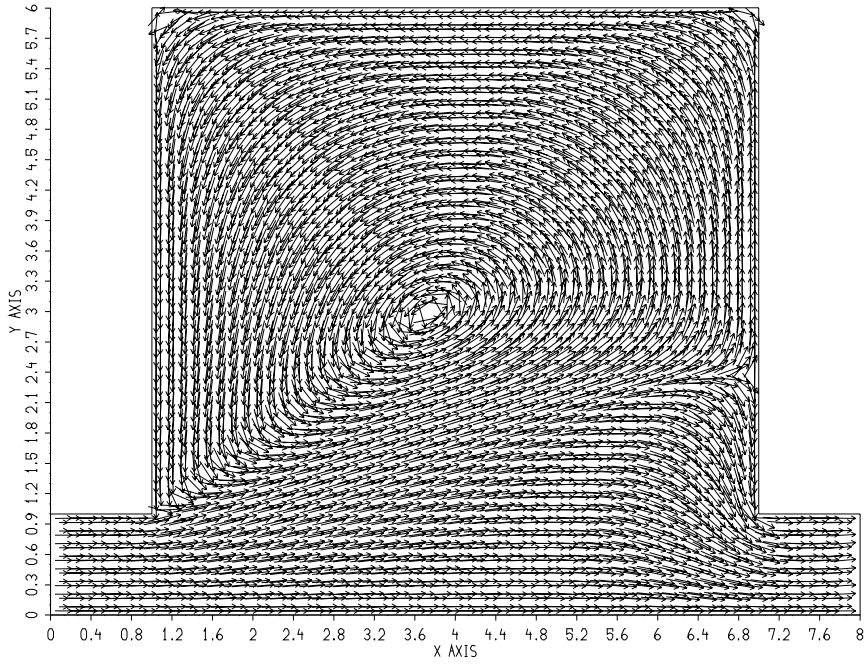

FIG. 5.3. *The $\alpha = 3/2$ flow field: a better approximation with $O(h^{3/2})$ artificial viscosity plus three corrections.*

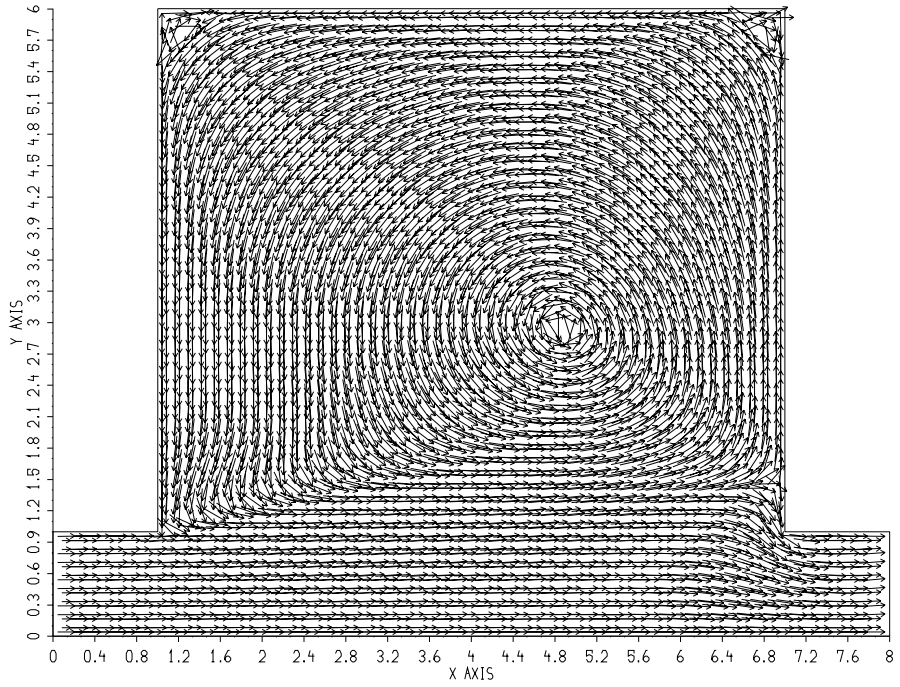

FIG. 5.4. *The $\alpha = 2$ flow field: $O(h^2)$ artificial viscosity plus three corrections yield the best resolution (uniform mesh).*

adaptive refinement we will therefore use $\alpha = 2$.

Next, Test Problem 5.2 was solved adaptively. Let $N(T)$ denote the number of triangles in the grid being considered for refinement. For a grid refinement threshold $C > 0$, a triangle T is refined if $Est_2^2(T) > C^2/N(T)$. If $Est_2^2(T) < C^2/2N(T)$, then T was marked for derefinement. We set $C_j = 1, j = 1, 2, 3$, and used a refinement threshold of $C = 4/10$. A Taylor–Hood finite element DCM discretization is used with $O(h^2)$ artificial viscosity on an r-Laplacian ($h^2|h\nabla \mathbf{u}^{j-1}|$) SGS model. The initial grid is shown in Figure 5.5, and every second grid obtained by the adaptive refinement procedure is shown in Figures 5.5–5.8.

Figure 5.8 shows the finest grid created by the adaptive refinement procedure. It contains approximately the same number of triangles (20,000) as the uniform grid in Figure 5.1. However, the adaptive refinement better resolves the regions of physical activity due to the concentration of triangles in these areas. Along the boundaries of the inflow and outflow pipe, refinement takes place because the residual term in the error estimator includes $\mathbf{u}\nabla\mathbf{u}$, which is large due to changes in the velocity especially near the outflow boundary. Further refinement is centered around a shear layer/separation curve which begins at the reentrant corner $(1, 1)$ and ends at a certain point along wall $\{(x, y): x = 7, y \in [1, 7]\}$. This line "separates" the fast flow through the pipe from the slower cavity flow. The velocity vector plot related to Figure 5.8 is shown in Figure 5.9. The plotting routine used sets all vectors to be of equal length in order to make the recirculating flow in the cavity clearly visible. This flow is much slower than the through flow and would hardly show up if vectors were scaled propor-

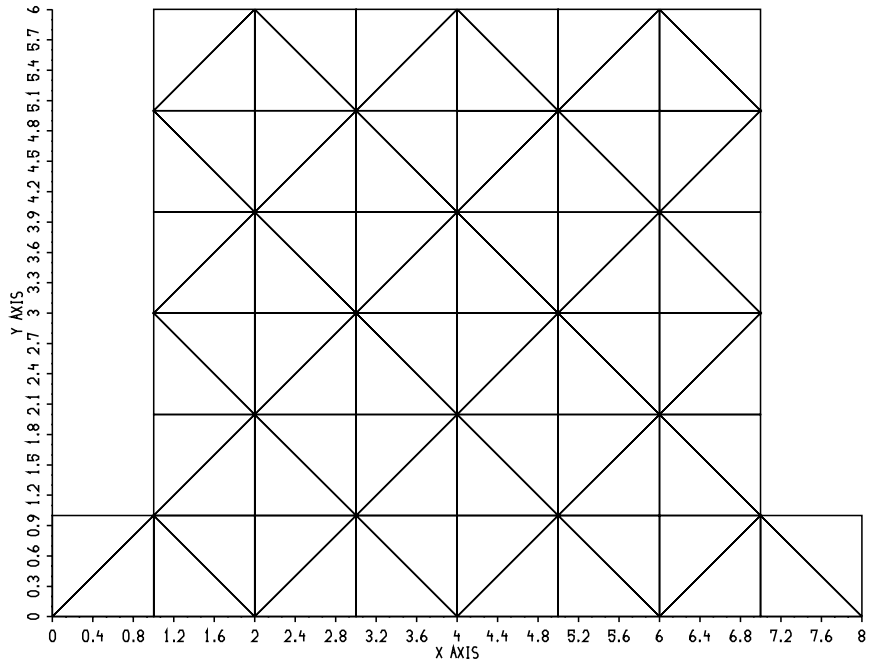

FIG. 5.5. *The initial grid for adaptive calculations.*

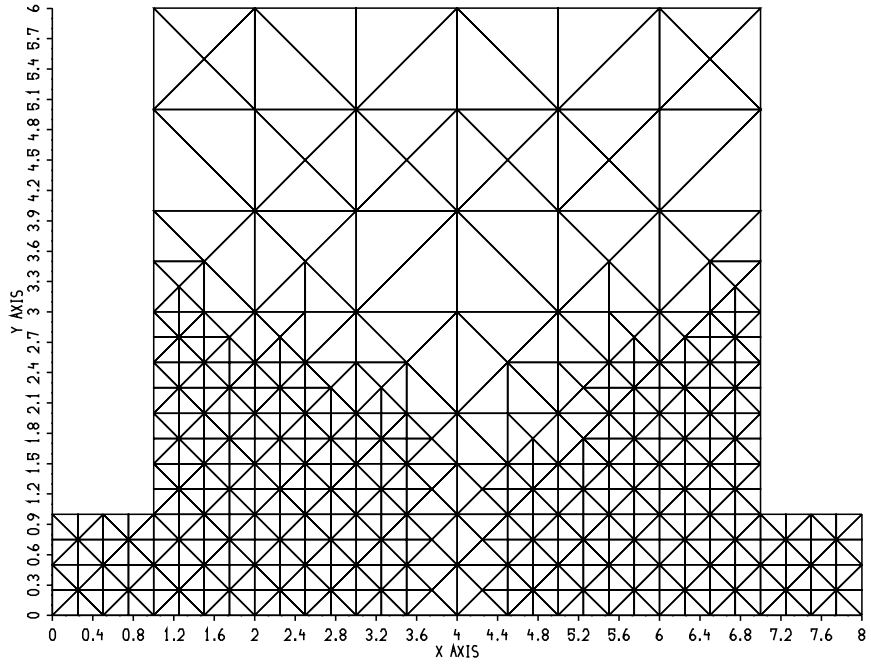

FIG. 5.6. *The second adaptively refined grid.*

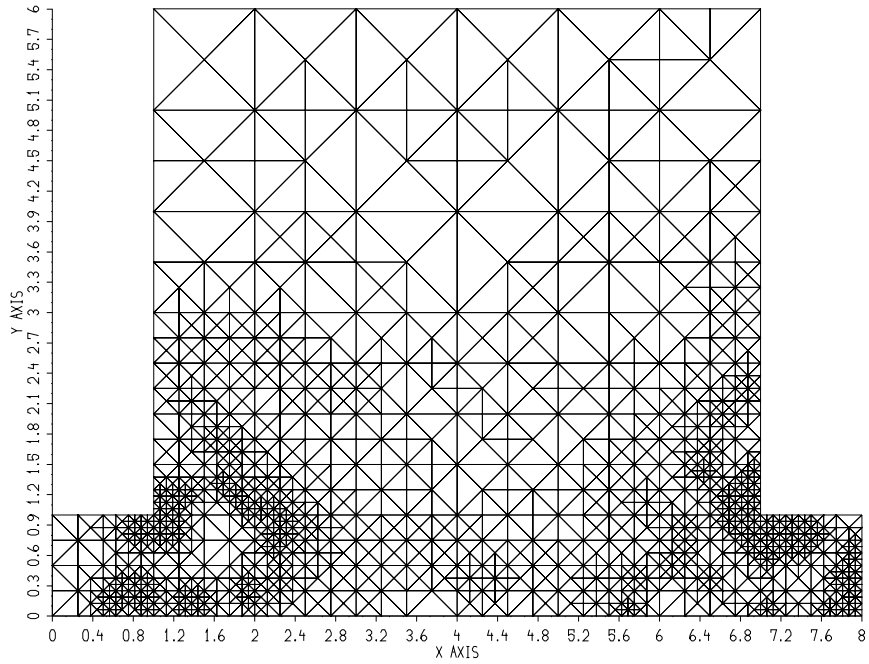

FIG. 5.7. *The fourth adaptively refined grid. Note the refinement in areas of large fluid stresses and at the approximate outflow boundary.*

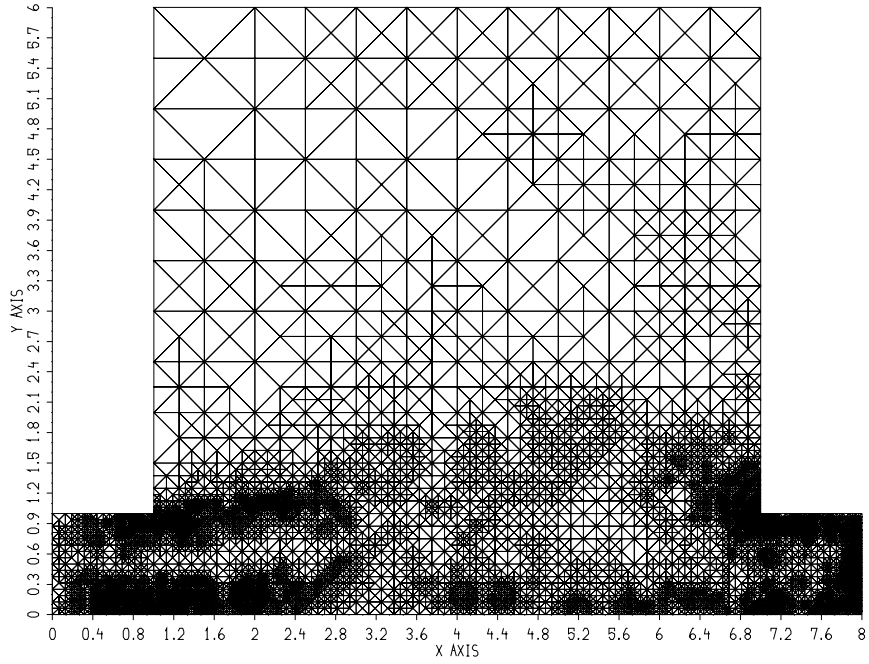

FIG. 5.8. *The sixth adaptively refined grid. Note the concentration of refinement in areas of physical activity.*

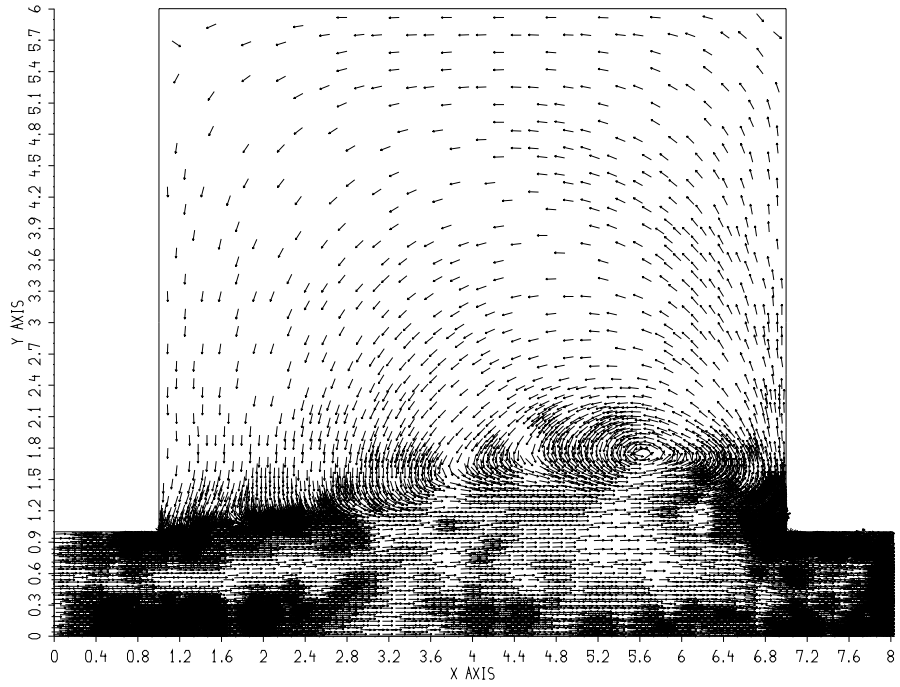

FIG. 5.9. *The flow field on the finest grid. All arrows are rescaled to be of equal size. A close-up view of the flow field in the right-hand corner follows.*

tional to their velocity. A magnification of the grid and related flow field is provided in Figures 5.10 and 5.11. These figures show that the shear layer connects to the boundary of the cavity at a point which is situated lower than in the case of the uniform refinement. Furthermore, the adaptive refinement picks up a small vortex in the outflow pipe. This recirculation region is an important physical structure.

The number of triangles $N(T)$ per grid G is shown in the third column of Table 5. The related number of degrees of freedom for the velocity and pressure combined, M, is given in the second column. Finally, the maximum amount of iterations needed to solve all nonlinear systems is given in the last column.

The subgridscale model used prevents nonphysical solutions caused by overcorrecting in the DCM. For instance, in computed approximate solutions to this problem without a SGS model we observed nonphysical eddies on the left-hand side which increased in number and decreased in size as the mesh was refined.

Adaptive defect correction discretizations show great promise for approximating flows of incompressible viscous fluids at higher Reynolds numbers. The method is especially attractive since it is easy to introduce a SGS model (or turbulence model) into the calculation without significantly increasing the cost of resolving the nonlinearity in the system.

The use of a posteriori error estimators and self-adaptive algorithms is especially promising when a SGS model is used in the discretization. Specifically, when the error is estimated with respect to solutions of the unperturbed Navier–Stokes equations, a SGS model can be used with impunity (i.e., without worries as to "modelling errors")

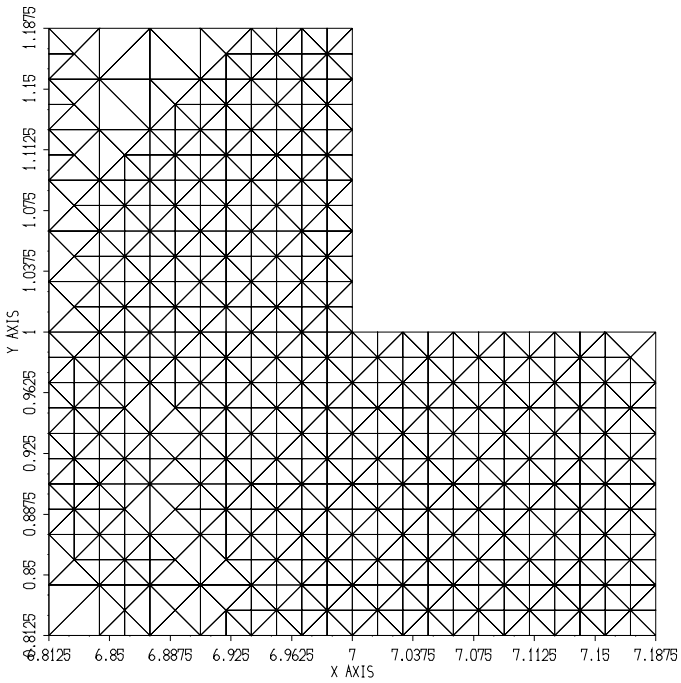

FIG. 5.10. *The shear layer down flow, grid magnification.*

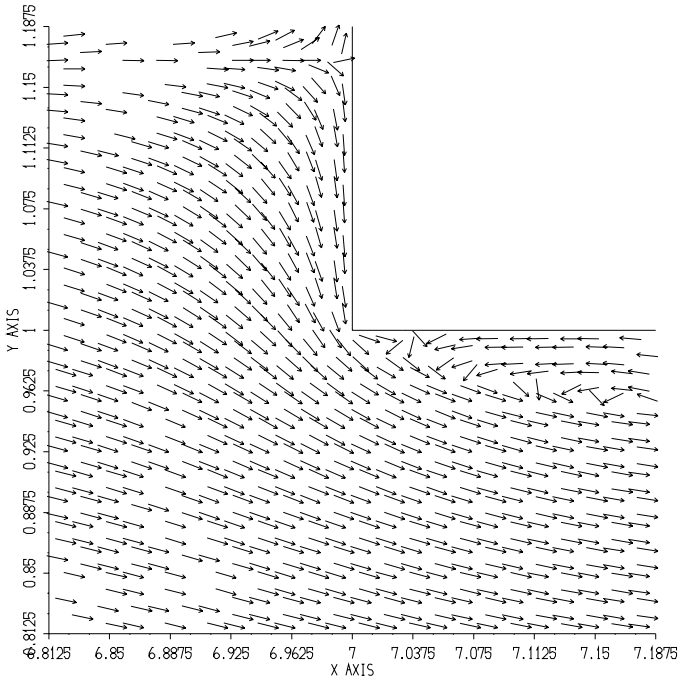

FIG. 5.11. *The shear layer down flow, flow field magnification. Note: a recirculating eddy is captured in this adaptive calculation (not in our uniform mesh simulation, nor in the k-ϵ simulations).*

TABLE 5.3
Degrees of freedom and number of Newton iterations ($\alpha = 2$).

G	M	$N(T)$	#Newton it.
0	1151	304	3
1	2393	646	4
2	5493	1512	4
3	17270	4831	5
4	43167	12180	4
5	116880	33150	2

to eliminate nonphysical eddies.

We highly recommend the pipe driven cavity (Test Problem 5.2) as a challenging test problem, similar in spirit to the driven cavity but perhaps more physically reasonable.

Based on the success of the adaptive DCMs herein, two natural questions arise for further study: (1) efficiency improvement of the method via, for instance, exact solvers and the elimination of the artificial viscosity step from one grid to the next; (2) analysis of the defect correction method applied at each time step in an evolutionary problem.

REFERENCES

[1] D.N., ARNOLD, F. BREZZI, AND M. FORTIN, *A stable finite element for the Stokes equations*, Calcolo, 21 (1984), pp. 337–344.

[2] O. AXELSSON, *A restarted version of a generalized preconditioned conjugate gradient method*, Commun. Appl. Numer. Methods, 4 (1988), pp. 521–530.

[3] O. AXELSSON, *Conjugate gradient type methods for unsymmetric and inconsistent systems of linear equations*, Linear Algebra Appl., 29 (1980), pp. 1–16.

[4] M. AINSWORTH AND J.T. ODEN, *A unified approach to a posteriori error estimation using element residual methods*, Numer. Math., 65 (1993), pp. 23–50.

[5] O. AXELSSON AND W. LAYTON, *Defect correction methods for convection dominated, convection diffusion equations*, RAIRO Modél. Math. Anal. Numér., 24 (1990), pp. 423–455.

[6] O. AXELSSON AND W. LAYTON, *Iterative methods as discretization procedures*, in Preconditioned Conjugate Methods, Lecture Notes in Math. 1457, O. Axelsson and Y. Lu. Kolotilina, eds., Springer-Verlag, Berlin, 1991, pp. 174–193.

[7] I. BABUŠKA AND W.C. RHEINBOLDT, *Error estimates for adaptive finite element computations*, SIAM J. Numer. Anal, 15 (1978), pp. 736-754.

[8] I. BABUŠKA AND A. MILLER, *A Posteriori Error Estimates and Adaptive Techniques for the Finite Element Method*, Tech. note BN-968, University of Maryland, Baltimore, MD, 1981.

[9] R.E. BANK AND A. WEISER, *Some a posteriori error estimators for elliptic partial differential equations*, Math. Comp., 44 (1985), pp. 283–301.

[10] K. BOHMER AND H.J. STETTER, *Defect Correction Methods—Theory and Applications*, Springer-Verlag, Berlin, 1984.

[11] B. CARDOT, B. MOHAMMADI, AND O. PIRONNEAU, *A few tools for turbulence models in Navier-Stokes equations*, in Incompressible Computational Fluid Dynamics, M.D. Gunzburger and R.A. Nicolaides, eds., Cambridge University Press, Cambridge, UK, 1993.

[12] PH. CLÉMENT, *Approximation by finite element functions using local regularization*, RAIRO Modél. Math. Anal. Numér., 2 (1975), pp. 77–84.

[13] G. COMTE-BELLOT, *Ecoulement turbulent entre deux paroix planes*, Technical report, Pub. Sci. et Tech. du Ministère de l'air, France, 1980.

[14] R.S. DEMBO, S.C. EISENSTAT, AND T. STEIHAUG, *Inexact Newton methods*, SIAM J. Numer. Anal., 19 (1982), pp. 400–408.

[15] D.A. DUNAVANT, *High degree efficient symmetrical Gaussian quadrature rules for the triangle*, Internat. J. Numer. Methods Engrg., 21 (1985), pp. 1291–1486.

[16] K. ERIKSSON AND C. JOHNSON, *Adaptive streamline diffusion finite element methods for stationary convection-diffusion problems*, Math. Comp., 60 (1993), pp. 167–188.

[17] V. Ervin and W. Layton, *High resolution, minimal storage algorithms for convection dominated, convection diffusion equations*, in Transactions of the Fourth Army Conference on Applied Mathematics and Computing, ARO Rep., 87-1, U.S. Army Res., Triangle Park, NC, 1987, pp. 1173–1201.

[18] V. Ervin and W. Layton, *A study of defect correction, finite difference methods for convection diffusion equations*, SIAM J. Numer. Anal., 26 (1989), pp. 169–179.

[19] M.E. Cawood, V.J. Ervin, W.J. Layton, and J.M. Maubach, *Adaptive defect correction methods for convection dominated, convection diffusion problems*, J. Comput. Appl. Math., to appear.

[20] V. Girault and P.-A. Raviart, *Finite Element Methods for Navier-Stokes Equations. Theory and Algorithms*, Springer-Verlag, Berlin, 1986.

[21] M. Gunzburger, *Finite Element Methods for Viscous Incompressible Flows. A Guide to Theory, Practice and Algorithms*, Academic Press, Boston, 1989.

[22] W. Hackbusch, *On multigrid iterations with defect correction*, in Multigrid Methods, Lecture Notes in Math. 960, W. Hackbusch and V. Trottenberg, eds., Springer-Verlag, Berlin, 1982, pp. 461–473.

[23] W. Hackbusch, *Multigrid Methods and Applications*, Springer-Verlag, Berlin, 1985.

[24] P. Hemker, *Mixed defect correction iteration for the accurate solution of the convection diffusion equation*, in Multigrid Methods, Lecture Notes in Math. 960, W. Hackbusch and V. Trottenberg, eds., Springer-Verlag, Berlin, 1982, pp. 485–501.

[25] P. Hemker, *An accurate method without directional bias for the numerical solution of a* 2*-D elliptic singular perturbation problem*, in Theory and Applications of Singular Perturbations, Lecture Notes in Math. 942, W. Eckhaus and E.M. de Jaeger, eds., Springer-Verlag, Berlin, 1982, pp. 192–206.

[26] P. Hemker and B Koren, *Defect correction and nonlinear multigrid for the steady Euler equations*, in Advances in Computational Fluid Dynamics, W.G. Habashi and M.M. Hafez, eds., Cambridge University Press, Cambridge, UK, 1992, pp. 273–291.

[27] P. Hemker and B. Koren, *Multigrid, defect correction and upwind schemes for the steady Navier-Stokes equations*, in Numer. Methods for Fluid Dynamics III, K.W. Morton and M.J. Baines, eds, Clarendon Press, Oxford, 1988.

[28] B. Koren, *Multigrid and Defect Correction for the Steady Navier-Stokes Equations, Applications to Aerodynamics*, C. W. I. Tract 74, Centrum voor Wiskunde en Informatica, Amsterdam, 1991.

[29] W. Layton, H.K. Lee, and J. Peterson, *Numerical solution of the stationary Navier-Stokes equations using a multi-level finite element method*, SIAM J. Sci. Comput., 20 (1998), pp. 1–12.

[30] W. Layton, *Solution algorithms for incompressible viscous flows at high Reynolds number*, Vestnik Moskov Univ. Ser. XV Vychisl. Mat. Kebernet., 1 (1996), pp. 25–35.

[31] W.J. Layton, *A nonlinear subgridscale model for incompressible viscous flow problems*, SIAM J. Sci. Comput., 17 (1996), pp. 347–357.

[32] J.M. Maubach, *Local bisection refinement for n-simplicial grids generated by reflections*, SIAM J. Sci. Comput., 16 (1995), pp. 210–227.

[33] J. Maubach, *The Amount of Similarity Classes Created by Local n-Simplicial Bisectionrefinement*, preprint, 1996.

[34] W.C. Rheinboldt and J.L. Liu, *A Posteriori Error Estimates for Parameterized Nonlinear Equation*, Institute for Computational Mathematics and Applications report 90-151, 1990.

[35] B. Mohammadi and O. Pironneau, *Analysis of the k-ϵ Turbulence Model*, Wiley, Chichester, UK, 1994.

[36] Y. Saad and M.H. Schultz, *GMRES: A generalized minimal residual algorithm for solving nonsymmetric linear systems*, SIAM J. Sci. Statist. Comput., 7 (1986), pp. 856–869.

[37] P. Sonneveld, *CGS, A fast Lanczos-type solver for nonsymmetric linear systems*, SIAM J. Sci. Statist. Comput., 10 (1989), pp. 36–52.

[38] H.J. Stetter, *The defect correction principle and discretization method*, Numer. Math., 29 (1978), pp. 425–443.

[39] A.H. Stroud, *Approximate Calculation of Multiple Integrals*, Prentice-Hall, New York, 1971.

[40] C. Taylor and P. Hood, *A numerical solution of the Navier-Stokes equations using the finite element method*, Comput. & Fluids, 1 (1973), pp. 73–100.

[41] M.J. Todd, *The Computation of Fixed Points and Applications*, Lecture Notes in Econom. and Math. Systems 124, Springer-Verlag, Berlin, 1976,

[42] S. Vanka, *Block-implit multigrid calculation of two-dimensional recirculating flows*, Comput. Methods Appl. Mech. Engrg., 59 (1986), pp. 29–48.

[43] R. Verfürth, *A Review of a Posteriori Error Estimation and Adaptive Mesh Refinement Techniques*, Wiley-Teubner, Chichester, UK, 1996.
[44] P.L. Viollet, *On the modelling of turbulent heat and mass transfers in computations of buoyancy affected flows*, in Proceedings of the International Conference on Numerical Methods for Laminar and Turbulent Flows, Venezia, 1981.
[45] O. Zienkiewicz, *The Finite Element Method in Engineering Science*, 3rd ed., McGraw-Hill, New York, 1977.